p-STAT3 influences doxorubicin and etoposide resistance of A549 cells grown in an *in vitro* 3D culture model

SIRIPORN KEERATICHAMROEN[1], THIWAREE SORNPRACHUM[1], LUKANA NGIWSARA[1], NARITTIRA ORNNORK[1] and JISNUSON SVASTI[1,2]

[1]Laboratory of Biochemistry, Chulabhorn Research Institute; [2]Applied Biological Sciences Program, Chulabhorn Graduate Institute, Bangkok 10210, Thailand

Received December 6, 2022; Accepted January 31, 2023

DOI: 10.3892/or.2023.8508

Abstract. Tumor microenvironment undoubtedly has a significant impact on therapeutic responses. Abundant evidence suggests that the 3D *in vitro* culture holds great promise for drug discovery and development by bridging the gap between conventional 2D culture and animal models. The present study described 3D basement membrane culture of A549 cells, which mimics the complex 3D arrangement of tumors *in vivo* and elucidates the underlying mechanisms of microenvironmental influences on cellular functions and therapeutic efficacy. A549 cells cultured in 3D undergo G_0/G_1 phase arrest and decreased migratory and invasive capacity, indicating dormant cell characteristics. Hypoxia, apoptosis and stemness were demonstrated in the A549 cells in 3D architecture compared with the 2D-cultured counterparts. More importantly, cells in the 3D environment exhibited increased resistance to different classes of anticancer agents. Western blotting revealed changes in the levels of key cancer-associated pathways, phosphorylated (p)-STAT3, p-ERK, and p-Akt, in response to 3D culture compared with 2D monolayer culture. Notably, mechanistic analysis using specific inhibitors showed that the STAT3 inhibitor overcomes the 3D culture-induced doxorubicin and etoposide resistance. These results implicated an important role of p-STAT3 in conferring chemoresistance in 3D-cultured A549 cells, as well as the use of STAT3 inhibitor as a potential chemosensitizer to improve drug sensitivity. Thus, 3D culture systems, that more closely resemble *in vivo* tumor biology, may be more effective models in searching for novel chemotherapeutic agents and therapeutic targets for cancer treatment.

Correspondence to: Dr Siriporn Keeratichamroen, Laboratory of Biochemistry, Chulabhorn Research Institute, 54 Kamphaeng Phet 6, Talat Bang Khen, Bangkok 10210, Thailand
E-mail: siriporn@cri.or.th

Key words: tumor microenvironment, drug resistance, STAT3, cancer therapy, three-dimensional culture

Introduction

Cancer, the malignant growth of cells due to uncontrolled cell proliferation, ranks as a major cause of morbidity and premature death worldwide. GLOBOCAN estimated that there were 18.1 million new cancer cases and nearly 10 million cancer deaths in 2020 (1). According to the World Health Organization (WHO), lung cancer is the leading cause of cancer mortality in 2020, accounting for 1.8 million deaths (2). The most common type of lung cancer is non-small cell lung cancer (NSCLC, including large cell carcinoma, squamous cell carcinoma and adenocarcinoma) which accounts for up to 85% of lung cancers, while small cell lung cancer is responsible for 10% of the cases and histological variants represent the other 5% (3). Cigarette smoking is the most prevalent risk factor for lung cancer. Other known contributory factors include radiation, radon gas, certain metals, smoke, toxic chemicals, asbestos, as well as genetic factors. Despite significant breakthroughs in the understanding of cancer biology, the success of current conventional chemotherapies remains limited due to toxicity, efficacy and drug resistance (4). Novel drug discovery and development is thus an important aspect of cancer research to improve outcomes in cancer treatment.

The discovery of new medications with remarkable effects has made significant progress and contributed significantly to disease-free survival improvement. However, drug resistance develops in the majority of patients, as treatment progresses. Chemotherapy resistance is a significant challenge to cancer treatment success and patient survival, resulting in cancer relapse and recurrence and, eventually, death. The ability of cancer cells to resist the effects of chemotherapeutic drugs can occur before treatment (intrinsic mechanisms) or later during treatment (acquired mechanisms). Drug resistance results from multiple molecular determinants, such as increased drug efflux, decreased drug uptake, alteration of drug targets, epigenetic alterations, increased DNA repair and inhibition of cell death (5). The high complexity and heterogeneity of tumors, as well as cancer's ability to evade therapies, render it more difficult to deal with drug resistance. There are several ongoing efforts towards improved understanding of the mechanisms of chemotherapy resistance and of developing novel therapeutic strategies to overcome it. Due to the high likelihood of drug resistance and treatment failure with

monotherapy, combination therapy regimens are preferred for overcoming chemotherapy resistance because they target multiple driver genes at once. Emerging evidence suggests that sequential chemotherapeutic administration may be more effective than combinational therapies in preventing drug resistance and increasing treatment success rates (6). One strategy for combating chemotherapy resistance is to target apoptotic pathways. An abundance of evidence suggests that natural compounds, such as galbanic acid, can induce TRAIL-mediated apoptosis (7). Specific drug delivery platforms, such as exosome or nanoparticle conjugations, have recently gained attention and demonstrated a remarkable potential to overcome drug resistance (8).

The tumor microenvironment (TME), a non-malignant part of tumors, has been widely implicated in tumor formation, progression and metastatic dissemination (9). In 2022, the hallmarks of cancer have been expanded from 6 to 14, with TME being recognized as the emerging participant in cancer development (10). Numerous studies have shown that the dynamic and bidirectional communication between cancer cells and the cellular (stromal cells) and acellular components (such as fibronectin, collagen, laminin and hyaluronan) in the TME can reprogram cancer initiation, growth, metastasis, as well as response to therapies (11).

Selection of the experimental model is the key to *in vitro* experimentation. Cell culture models that perform similarly, both morphologically and functionally, to the cells *in vivo* are desirable, in order to obtain the most reliable results. Currently, the traditional two-dimensional (2D) culture system, where cells are cultured as monolayers on plastic surfaces, serves as the main platform for basic cellular research. However, important signals from the TME, particularly factors influencing response to therapy are largely ignored when cells are cultured in 2D. Thus, the failure of 2D cultures to imitate the complexity of *in vivo* microenvironment may be responsible for the poor correlation between *in vitro* and *in vivo* drug candidate activity by providing misleading results and non-predictive data (12). Although the vast majority of new therapeutic agents show excellent antitumor properties *in vitro*, only 5% of the compounds passed clinical trials, indicating that 2D culture is a relatively poor model for drug discovery and development (13).

It is increasingly evident that three-dimensional (3D) cell culture systems represent improved predictive *in vitro* approaches than the traditional 2D culture. 3D culture models can more accurately reflect the complex interactions of cell-cell and cell-extracellular matrix (ECM) interactions that resemble *in vivo* microenvironment, thus providing more accurate results for preclinical drug development. These interactions, as well as the 3D architecture affect a range of cellular functions and cell behavior, including morphology, proliferation, differentiation, angiogenesis, migration, invasion and gene/protein expression (14,15). Moreover, several recent publications demonstrated that numerous signaling pathways associated with drug sensitivity are differentially activated in cells cultured in 3D compared with 2D settings, leading to increased drug resistance in 3D culture (16,17). Notably, numerous studies have shown that the gene or protein expression patterns of 3D-cultured cells more closely resemble those of native tissue than those of monolayer cultures (18,19).

In the present study, the culture of A549 human lung epithelial cells in a basement membrane extract-based 3D culture system was described, that restored the crucial microenvironmental cues from the ECM and provided a more physiologically relevant model. Cellular characteristics of cells in 2D and 3D culturing microenvironment which are key determinants in cancer progression including migration, invasion, cell cycle, hypoxia, stemness and degree of apoptosis, were evaluated. Chemotherapeutic response of cells to a variety of conventional chemotherapeutic drugs, small molecule inhibitors, and natural products was also assessed. Further investigation of the signaling events accounting for the biological features of cells led to the delineation of key regulatory elements associated with tumor dormancy and drug resistance.

Materials and methods

Cell culture. The human lung epithelial cell line A549 (cat. no. CCL-185™; American Type Culture Collection) was maintained in RPMI-1640 containing 10% (v/v) FBS (Gibco; Thermo Fisher Scientific, Inc.) and 1% (v/v) antibiotic-antimycotic solution (Gibco; Thermo Fisher Scientific, Inc.). The 3D on-top culture was performed as previously described (20) with certain modifications. Briefly, the prechilled 24-well culture plates were coated with a thin layer of reconstituted basement membrane (Matrigel; BD Biosciences, cat. no. 356234) and incubated at 37˚C for 30 min. Subsequently, a cell suspension ($0.5x10^5$ cells in 500 μl of complete medium containing 2% Matrigel) was added on top of Matrigel. The medium was changed every 3-4 days and the cultures were maintained for 7 days. For 2D cultivation, the cells were cultured for 3 days before being used. In all experiments, the cells were maintained in a humidified atmosphere incubator (5% CO_2) at 37˚C.

Flow cytometric analysis of apoptosis and cell cycle distribution. The apoptotic profiles and cell cycle progression of A549 cells cultured in 2D/3D culturing microenvironments were assessed using Muse® Cell Analyzer (Luminex) as previously described (21). Briefly, the cells were harvested, dissociated into single-cell suspensions and stained with Muse Annexin V & Dead Cell kit or Muse Cell Cycle kit (Luminex), according to the manufacturer's instructions. Then, the cells were subjected to apoptotic detection or cell cycle analysis. Results are expressed as the mean values of total apoptosis (percentage of early + late apoptotic cells) or proportion of the cells in each phase of cell cycle (G_0/G_1, S and G_2/M).

In vitro cell migration and invasion assays. Cellular potential for migration and invasion of the 2D and 3D cells were assessed using 24-well Transwell chambers (8 mm; BD Biosciences). For migration assay, a total of $4x10^4$ cells in 200-μl suspension were seeded into the Transwell chamber, while $1x10^5$ cells were seeded in the Matrigel-coated upper chamber for the invasion assay. The lower compartment of the chamber was filled with 500 μl of chemoattractant [conditioned medium prepared from human lung fibroblasts (MRC-5)]. The cells were allowed to migrate or invade for 24 h, after which the non-migratory or non-invasive cells on the top of the filter were carefully removed with cotton swabs. Membrane containing migratory

or invasive cells was immersed in 25% methanol for 15 min, developed with 500 μl of 0.5% crystal violet (MilliporeSigma) for 15 min, and acid-extracted with 100 μl of 0.1 N HCl in methanol. The absorbance was measured at 550 nm using a microplate reader.

Drug sensitivity assay. The chemosensitivity of the cells to a variety of conventional chemotherapeutic drugs, small molecule inhibitors, and natural products was determined using an MTT assay. The choice of chemotherapeutic agents was motivated by the desire to compare cell response between two models, 3D cells in the present study and semi-solid Matrigel-embedded cells in our previous study (22). Standard chemotherapeutic agents that target proliferating cell mechanisms, as well as drugs with multi-targeted actions that do not rely on the proliferative status of the cells, were used. Doxorubicin, etoposide, vinblastine, paclitaxel, 2-deoxyglucose (2-DG), emodin, apigenin, resveratrol, caffeic acid phenethyl ester (CAPE), curcumin, capsaicin, shikonin, and dihydroxybenzaldehyde (DHBZ) were purchased from MilliporeSigma. Cucurbitacin I (CBC-I), AG-490, and BAY 11-7085 were purchased from Calbiochem. Chrysin was kindly provided by Dr Sirivan Athikomkulchai (Faculty of Pharmacy, Srinakharinwirot University, Nakhon Nayok, Thailand). Briefly, 100 μl of the cell suspension was seeded into each well of a 96-well plate ($1x10^4$ cells), then 100 μl of cytotoxic agents in a range of concentrations or a vehicle (cell culture media) were added. After 48 h of incubation, each well was replaced with 100 μl of 0.5 mg/ml MTT solution (MilliporeSigma) and incubated for another 2 h at 37˚C. Absorbance was measured at 550 nm (650 nm was subtracted as the reference wavelength) using a microplate reader. The IC_{50} value for each cytotoxic drug (the drug concentration exhibiting 50% cell viability) was calculated.

Reverse transcription-quantitative PCR (RT-qPCR) analysis. Total RNA isolation was performed using NucleoSpin RNA Mini kit, following the manufacturer's instructions. First strand cDNA was reverse transcribed form 2 μg of template RNA using SuperScript III Reverse Transcriptase (Invitrogen; Thermo Fisher Scientific, Inc.). A total of 1 μl of 10 mM Oligo$(dT)_{20}$ primer and 2 μg RNA were combined and the volume was adjusted to 12 μl with DEPC-treated water in a 0.2 ml PCR tube. The tube was incubated at 60˚C for 5 min and then placed on ice immediately. Meanwhile, a master reaction was prepared with 4 μl 5X First-Strand Buffer, 1 μl 0.1 M DTT, 1 μl 10 mM dNTP mix, and 1 μl SuperScript™ III RT (200 units/μl) and added to the reaction. The reaction was incubated at 50˚C for 50 min, followed by inactivation of the reaction by heating at 70˚C for 15 min. Real-time PCR was performed using StepOnePlus™ Real-Time PCR System (Applied Biosystems; Thermo Fisher Scientific, Inc.). Each PCR reaction (20 μl) was composed of 20 ng of cDNA, KAPA SYBR FAST qPCR kit reagent (Kapa Biosystems; Roche Diagnostics) and 10 pmol of PCR primers. Oligonucleotide primers used in the present study are listed in Table I. The thermocycling conditions were as follows: An initial activation step at 95˚C for 10 min was followed by 40 cycles comprising denaturation at 95˚C for 15 sec, annealing at 60˚C for 30 sec, and extension at 72˚C for 30 sec. Data were analyzed using

Table I. Sequence of primers used for reverse transcription-quantitative PCR analysis.

Gene name	Primer sequence (5'→3')
uPA	F: TCGTCTGTTCCCTCCAAGGC
	R: TGCGGATCCAGGGTAAGAAG
uPA receptor	F: TAAGACCAACGGGGATTGCC
	R: TCTCCTTCTTCCCACAAGCG
c-MET	F: CATGCCGACAAGTGCAGTA
	R: TCTTGCCATCATTGTCCAAC
MMP-1	F: AGAGCAGATGTGGACCATGC
	R: TTGTCCCGATGATCTCCCCT
MMP-2	F: CAAGGACCGGTTCATTTGGC
	R: GGCCTCGTATACCGCATCAA
MMP-3	F: ACAAAGGATACAACAGGGACCA
	R: AGCTTCAGTGTTGGCTGAGT
MMP-7	F: AGTGGTCACCTACAGGATCG
	R: GGGATCTCTTTGCCCCACAT
MMP-9	F: AAGGATGGGAAGTACTGGCG
	R: GCTCCTCAAAGACCGAGTCC
MMP-10	F: AGTTTGGCTCATGCCTACCC
	R: TTGGTGCCTGATGCATCTTCT
MMP-11	F: ACCTTTACTGAGGTGCACGAG
	R: CAAATTCATGGGCTGCCACC
MMP-13	F: TCCAGTCTCTCTATGGTCCAGG
	R: CCTCGGAGACTGGTAATGGC
TIMP-1	F: GCTGTGAGGAATGCACAGTGTT
	R: CCTTTTCAGAGCCTTGGAGGA
TIMP-2	F: GTTTATCTACACGGCCCCCT
	R: TCGGCCTTTCCTGCAATGAG
TIMP-3	F: ACCGAGGCTTCACCAAGATG
	R: ATAGACGCGACCTGTCAGCA
TIMP-4	F: AACTGTGGCTGCCAAATCAC
	R: GCTTTCGTTCCAACAGCCAG
TUBBI	F: ATACCTTGAGGCGAGCAAAA
	R: CTGATCACCTCCCAGAACTTG
TUBBIIA	F: AAATATGTACCTCGGGCCATC
	R: GTTATTCCCGGCTCCACTCT
TUBBIIB	F: AGGACGGACAGACCCAGAC
	R: CTGATGACCTCCCAAAACTTG
TUBBIII	F: GCAACTACGTGGGCGACT
	R: CGAGGCACGTACTTGTGAGA
TUBBIVA	F: CCGGACAACTTCGTGTTTG
	R: ACAGCGTCCACCAGCTCT
TUBBIVB	F: TTGTCTACTTCCTCCTGCTTCC
	R: CTGATCACCTCCCAAAACTTG
TUBBV	F: AGGCTACGTGGGAGACTCG
	R: GCCCTGGGCACATATTTCT
TUBBVI	F: GGATGCGTGAAATTGTCCAT
	R: AGTCGATCCCGTGTTCCTC
MDR-1	F: GTCTTTGGTGCCATGGCCGT
	R: ATGTCCGGTCGGGTGGGATA
MRP-1	F: CTGACAAGCTAGACCATGAATGT
	R: CCTTTGTCCAAGACGATCACCC

Table I. Continued.

Gene name	Primer sequence (5'→3')
MRP-2	F: GCCAGATTGGCCCAGCAAA
	R: AATCTGACCACCGGCAGCCT
MRP-3	F: GGGACCCTGCGCATGAACCTG
	R: TAGGCAAGTCCAGCATCTCTGG
MRP-5	F: CTAGAGAGACTGTGGCAAGAAGAGC
	R: AAATGCCATGGTTAGGATGGC
MRP-7	F: TAGGCACTGACTCTGAACGG
	R: TTGTTGACGGGTACCAGCAG
BCRP	F: TGGCTGTCATGGCTTCAGTA
	R: GCCACGTGATTCTTCCACAA
LRP	F: GAGCAGTTCACAGTGTTGTCC
	R: AAAGCCAAAGACAGCAGTGCG
HIF-1a	F: ATCCATGTGACCATGAGGAAATG
	R: CTCGGCTAGTTAGGGTACACTT
Oct4A	F: CGCAAGCCCTCATTTCAC
	R: CATCACCTCCACCACCTG
Oct4B	F: CAGGGAATGGGTGAATGAC
	R: AGGCAGAAGACTTGTAAGAAC
Oct4B1	F: GGGTTCTATTTGGTGGGTTCC
	R: TCCCTCTCCCTACTCCTCTTCA
Nanog	F: ATGCCTCACACGGAGACTG
	R: CTGCGTCACACCATTGCTA
CD133	F: GCTTTGCAATCTCCCTGTTG
	R: TTGATCCGGGTTCTTACCTG
EPCAM	F: CGCAGCTCAGGAAGAATGTG
	R: TGAAGTACACTGGCATTGACGA
Sox-2	F: CAAGATGCACAACTCGGAGA
	R: GCTTAGCCTCGTCGATGAAC
ALDH1	F: TCCTGGTTATGGGCCTACAG
	R: CTGGCCCTGGTGGTAGAATA
RPS13	F: CGAAAGCATCTTGAGAGGAACA
	R: TCGAGCCAAACGGTGAATC

the $2^{-\Delta\Delta Cq}$ method (23). The relative mRNA expression of the gene was normalized to the level of RPS13 mRNA (internal control).

Western blot analysis. A549 cells cultured in 2D monolayer or 3D aggregates were harvested and lysed in cell signaling lysis buffer (Merck Millipore) containing protease/phosphatase inhibitor cocktail (Cell Signaling Technology, Inc.). Protein quantification was performed using a Bradford assay kit (Bio-Rad Laboratories, Inc.). A total of 20 μg protein per lane was separated by 10% SDS-PAGE, electroblotted onto Immobilon-P Transfer Membranes (Merck Millipore) and blocked for 1 h at room temperature with 3% BSA (Sigma-Aldrich; Merck KGaA) in TBS-T (0.1% Tween-20). The membranes were then probed with the indicated primary antibodies: phosphorylated (p)-STAT3 (Y705; 1:250; rabbit, monoclonal; cat. no. 9145), STAT3 (1:3,000; rabbit, polyclonal; cat. no. 4904), p-Akt (1:250; rabbit, polyclonal; cat. no. 9271), Akt (1:1,000; rabbit, polyclonal; cat. no 9272), p-ERK (1:10,000; rabbit, polyclonal; cat. no. 9101), ERK (1:4,000; rabbit, polyclonal; cat. no. 9102), p-p38 (T180/Y182; 1:250; rabbit, polyclonal; cat. no. 9211), p38 (1:1,000; rabbit, polyclonal; cat. no. 9212), p-FAK (1:200; rabbit, monoclonal; cat. no. 8556), FAK (1:1,000; rabbit, polyclonal; cat. no. 3285), Mcl-1 (1:250; rabbit, polyclonal; cat. no. 4572), survivin (1:200; rabbit, polyclonal; cat. no. 2803), puma (1:500; rabbit, polyclonal; cat. no. 4976), cyclin D1 (1:250; rabbit, polyclonal; cat. no. 2922), cyclin D3 (1:1,000; mouse, monoclonal; cat. no. 2936), CDK2 (1:1,000; rabbit, monoclonal; cat. no. 2546) (all from Cell Signaling Technology, Inc.), MYLK (1:200; mouse, monoclonal; cat. no. sc-365352; Santa Cruz Biotechnology, Inc.) and GAPDH (1:50,000; rabbit, monoclonal; cat. no. ab190480; Abcam) at 4˚C overnight. The membranes were washed and incubated for 1 h at room temperature in a 1:5,000 dilution of HRP-conjugated goat anti-rabbit (monoclonal; cat. no. 7074; Cell Signaling Technology, Inc.) or rabbit anti-mouse (polyclonal; cat. no. P0260; Dako; Agilent Technologies, Inc.) secondary antibodies. Visualization of the protein bands was performed with the SuperSignal™ West Pico PLUS Chemiluminescent Substrate (cat. no. 34580; Thermo Fisher Scientific) or SuperSignal™ West Femto Maximum Sensitivity Substrate (cat. no. 34096; Thermo Fisher Scientific, Inc.). Quantification of the bands was carried out by densitometry using ImageJ version 1.53k software (National Institutes of Health).

Statistical analysis. All experimental data were expressed as means ± standard deviation of three biological replicates. Statistical values were performed using a two-tailed unpaired Student's t-test to determine the difference between 2 groups. The statistical significance between multiple experimental groups was assessed using one-way analysis of variance (ANOVA), followed by Tukey's post hoc test. $P<0.05$ was considered to indicate a statistically significant difference.

Results

Morphological characteristics of A549 cells in 2D and 3D-cultivation. Cell morphology was assessed on day 0, 2, 4, 7, and 9 using inverted phase-contrast microscopy. As revealed in Fig. 1, the morphologies of the cells differed noticeably between the two culturing strategies. A549 cells plated on tissue culture plastic for 2D culture appeared flat and preserved the typical cobblestone form (Fig. 1, left panel), whereas the shape of cells plated on Matrigel for 3D culture was changed to be spherical, similar to acini *in vivo* (Fig. 1, right panel). The 7-day cultivation period was chosen for the 3D culture approach based on previous experience with excessive 3D aggregate compaction leading to cell death.

A549 cells cultured as 3D aggregates undergo apoptosis. Several studies suggested that in 3D cultures, gradients of oxygen and nutrients as well as the accumulation of waste led to cell death, which increases with prolonged culture time (24,25). In the present study, Annexin V/7-AAD double staining and flow cytometry allowed quantitative measurement of apoptosis in 2D and 3D culturing systems. As demonstrated in Fig. 2, a higher percentage of cells cultured

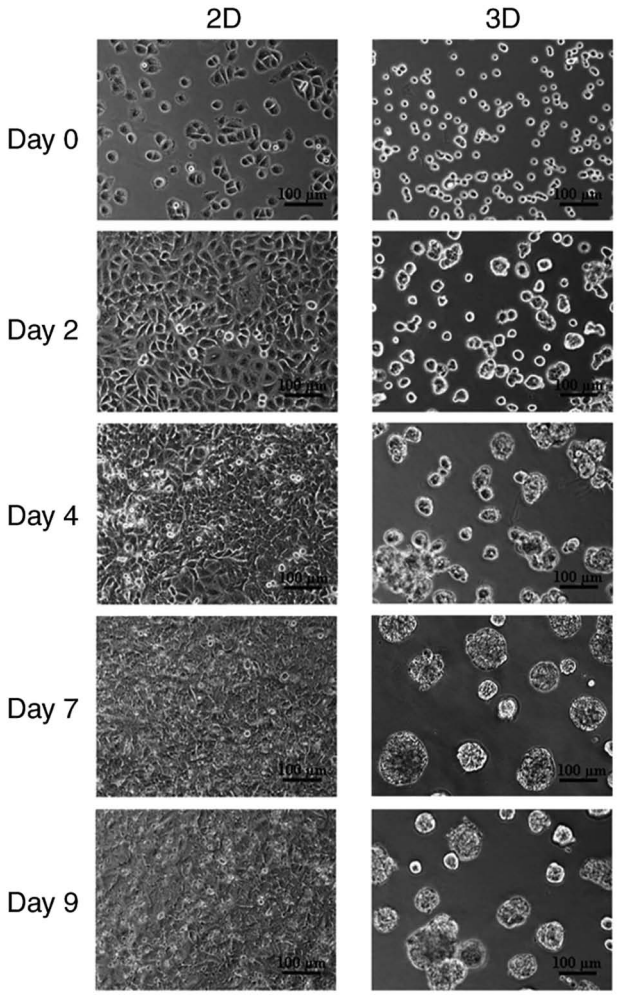

Figure 1. Morphological assessments of A549 cells in 2D and 3D culturing systems. Phase-contrast images of A549 cells cultured as a monolayer on plastic plates (left panels) and clustered morphology of the cells in the 3D on-top culture (right panels). Magnification, x200. Scale bar, 100 μm.

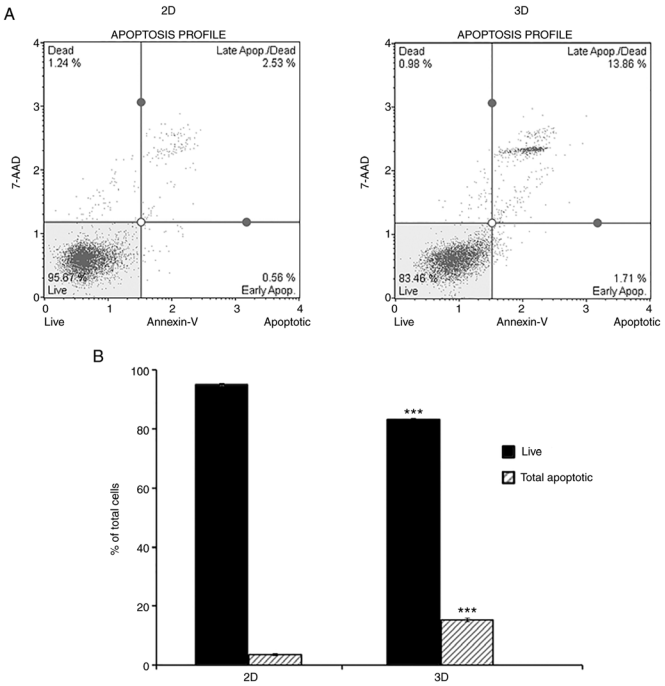

Figure 2. Annexin V/7-AAD double staining for apoptosis detection. (A) Representative dot plots showing Annexin V/7-AAD double staining of A549 cells cultured in 2D culture (left) and 3D culture (right). (B) Quantitative analysis of the percentages of live cells and total apoptotic cells. ***P<0.001 vs. 2D.

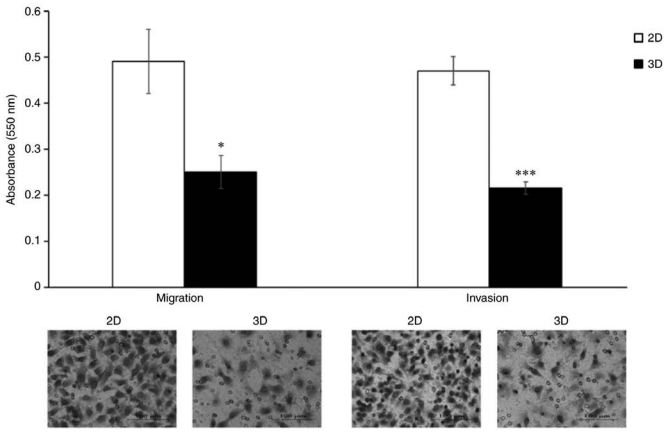

Figure 3. Cell migration and invasion assay. The results of Transwell migration and invasion assays for A549 cells following 2D and 3D culture, with bar graphs showing quantification of the migratory and invasive cells. *P<0.05 and ***P<0.001 vs. 2D. Magnification, x200. Scale bar, 100 μm.

in 3D (15.2±0.6%) stained positive for Annexin V compared with the 2D culture (3.5±0.4%), indicating increased apoptosis of cells in the 3D model.

Effect of 3D culture on cell migration and invasion. Migratory and invasive behavior of A549 cells under 2D and 3D culture were evaluated using the Transwell cell migration and invasion assay. The attenuation of the migration and invasion ability of A549 cells following 3D-cultivation are revealed in Fig. 3. Cell migration ability was significantly lower in the 3D model than that in the 2D model, with the number of migrating cells being 49% lower among cells cultured in 3D. Similar results were observed in the Transwell Matrigel invasion assay, where 3D *in vitro* culture reduced the invasive ability of A549 cells to 46% compared with those cultured in 2D.

The 3D culture system induces G_0/G_1 phase arrest in A549 cells. The effect of 3D culture on A549 cell cycle progression was investigated by flow cytometric analysis. The results demonstrated a significantly larger proportion of cells in the G_0/G_1 phase in 3D-cultured A549 cells compared with the corresponding 2D monolayer cultures (79.5±1.3 vs. 57.3±1.3%; Fig. 4). Consistent with this result, the 3D-cultured A549 cells exhibited a decrease in the percentage of cells in the S phase (3.8±0.4%) and G_2/M phase (16.6±0.9%), compared with the traditional 2D monolayer (9.7±0.4 and 32.7±1.2%, respectively). These findings revealed that cell cycle arrest at the G_0/G_1 phase was induced in A549 cells cultured in 3D.

Differential response of 2D and 3D cultured A549 cells to chemotherapy. The differences in cell responsiveness to various chemotherapeutic agents between 2D and 3D cultivation were investigated. Cells cultured in 2D and 3D were harvested, dissociated into individual cells and exposed to various concentrations of the drugs. The survival rate was

Table II. Chemosensitivity of 2D- and 3D-cultured A549 cells against various anticancer agents.

Anticancer agents	IC_{50}		Fold change	P-value
	2D	3D		
Doxorubicin (μM)	0.8±0.0	18.7±2.6	24.5±4.2	0.0006
Etoposide (μM)	24.3±2.4	545.0±14.7	22.6±1.7	$1.005x10^{-6}$
2-DG (mM)	5.6±1.0	78.3±6.2	14.6±3.3	$8.354x10^{-5}$
CBC-I (μM)	0.1±0.0	1.0±0.2	10.5±1.3	0.003
Emodin (μM)	35.0±3.2	131.7±7.4	3.8±0.1	$7.105x10^{-5}$
Vinblastine (nM)	27.7±2.8	84.0±5.3	3.1±0.2	0.0002
Paclitaxel (nM)	11.3±1.2	33.3±2.6	3.0±0.2	0.0004
Apigenin (μM)	34.8±5.4	84.8±19.2	2.5±0.8	0.024
Resveratrol (μM)	88.7±2.6	176.7±11.9	2.0±0.2	0.0005
AG-490 (μM)	59.8±4.4	121.7±16.5	2.0±0.3	0.007
CAPE (μM)	60.8±2.7	113.3±12.5	1.9±0.1	0.004
Curcumin (μM)	27.7±2.1	51.0±9.9	1.8±0.2	0.031
Shikonin (μM)	1.8±0.0	3.2±0.3	1.8±0.2	0.004
Chrysin (μM)	66.8±4.5	104.3±18.9	1.6±0.2	0.052
DHBZ (μM)	567.7±32.3	730.0±78.7	1.3±0.1	0.054
Capsaicin (μM)	181.7±2.4	215.0±7.1	1.2±0.0	0.003
Bay 11-7085 (μM)	15.9±2.8	16.8±0.6	1.1±0.2	0.665

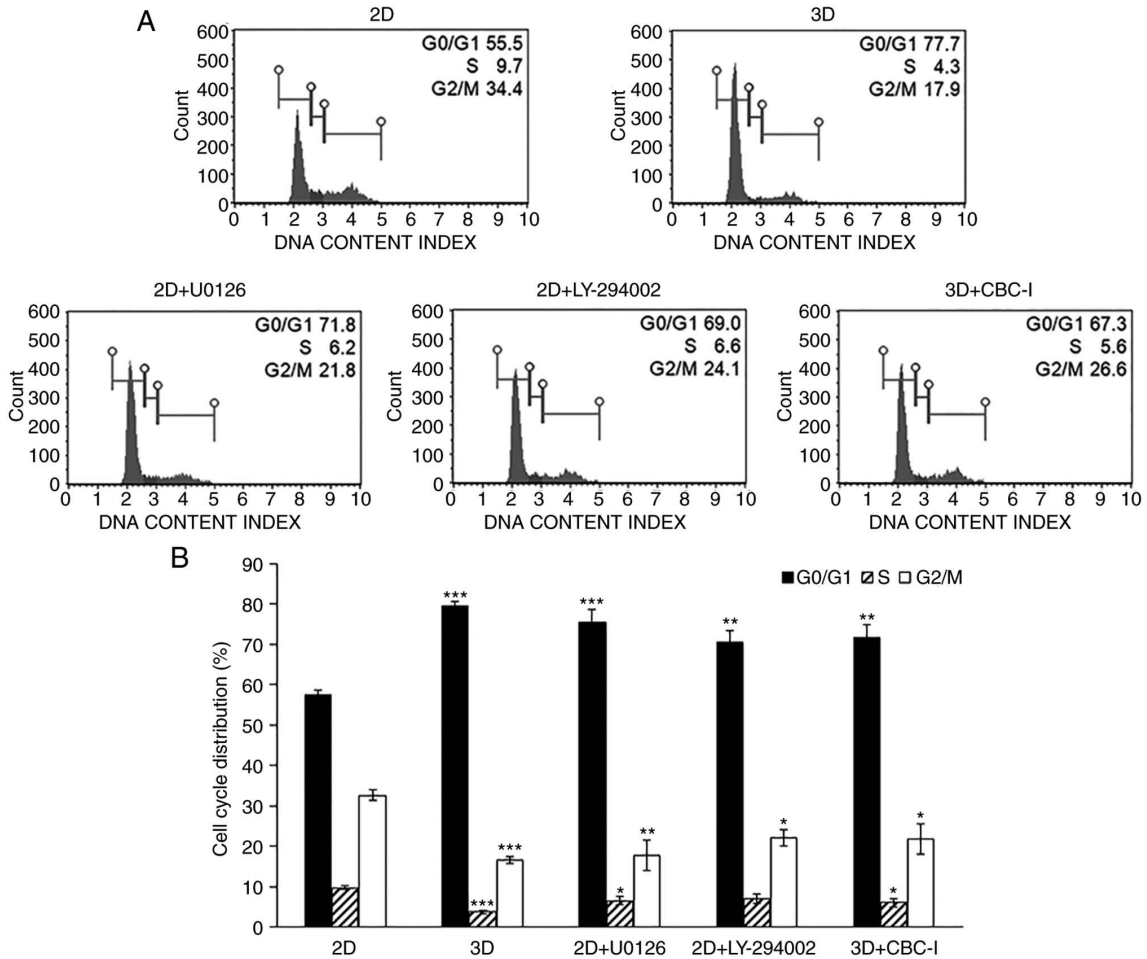

Figure 4. Analysis of A549 cell cycle distribution. (A) Representative cell cycle profiles of A549 cells in 2D and 3D models, as well as after treatment with specific inhibitors. (B) Histograms showing the effects of culturing system and specific inhibitors on the percentages of A549 cells in the G_0/G_1, S, and G_2/M phase. *P<0.05, **P<0.01 and ***P<0.001 vs. 2D.

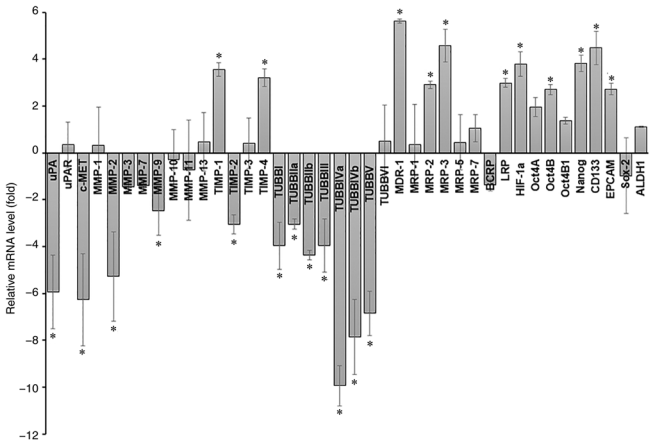

Figure 5. Reverse transcription-quantitative PCR gene expression analysis of A549 cells cultured in 2D and 3D systems. Results show relative mRNA expression of an array of genes associated with tumor progression and metastasis, drug resistance, hypoxia-associated protein, and stemness marker. Data are expressed as fold differences compared with 2D cells. The comparative $2^{-\Delta\Delta Cq}$ method (normalized to the expression of the RPS13 reference gene) was used to determine the relative level of gene expression. *, significant difference (≥2.5-fold) vs. 2D.

determined after 48 h of incubation by MTT assays (Fig. S1). The results demonstrated that the 3D cells display enhanced resistance to a number of anticancer agents [doxorubicin (24.5-fold), etoposide (22.6-fold), 2-DG (14.6-fold), CBC-I (10.5-fold), emodin (3.8-fold), vinblastine (3.1-fold) and paclitaxel (3.0-fold)], using a threshold value of 3-fold difference (Table II).

Differences in gene expression levels of A549 cells in 2D and 3D culture. To gain insights into the molecular mechanisms underlying the effects of the culturing system, the alterations in gene expression patterns of A549 cells cultured under 2D and 3D culture were examined by RT-qPCR. An array of genes associated with tumor progression and metastasis [uPA, uPA receptor (uPAR), c-MET, MMP-1, MMP-2, MMP-3, MMP-7, MMP-9, MMP-10, MMP-11, MMP-13, TIMP-1, TIMP-2, TIMP-3, TIMP-4, and beta-tubulin isotypes (TUBBI, TUBBIIa, TUBBIIb, TUBBIII, TUBBIVa, TUBBIVb, TUBBV, and TUBBVI)], drug resistance (MDR-1, MRP-1, MRP-2, MRP-3, MRP-5, MRP-7, BCRP, and LRP), hypoxia-associated protein (HIF-1a), and stemness marker (Oct4A, Oct4B, Oct4B1, Nanog, CD133, EPCAM, Sox-2, and ALDH1) was assessed. Using a 2.5-fold change in expression as a threshold value, the results demonstrated that 11 genes were upregulated [TIMP-1 (3.5-fold), TIMP-4 (3.2-fold), MDR-1 (5.6-fold), MRP-2 (2.9-fold), MRP-3 (4.6-fold), LRP (3.0-fold), HIF-1a (3.8-fold), Oct4B (2.7-fold), Nanog (3.8-fold), CD133 (4.5-fold) and EPCAM (2.7-fold)] and 12 genes were downregulated [uPA (-5.9-fold), c-MET (-6.3-fold), MMP-2 (-5.3-fold), MMP-9 (-2.5-fold), TIMP-2 (-3.1-fold), TUBBI (-4.0-fold), TUBBIIa (-3.1-fold), TUBBIIb (-4.4-fold), TUBBIII (-4.0-fold), TUBBIVa (-9.9-fold), TUBBIVb (-7.9-fold), and TUBBV (-6.9-fold)] in A549 cells cultured in 3D compared with baseline expression of corresponding 2D monolayer cultures (Fig. 5).

Effect of 3D in vitro culture on protein expression. The signaling molecules linked to cell survival, proliferation, stress, migration, apoptosis and cell cycle were evaluated for protein expression levels by Western blot analysis. As shown in Fig. 6, A549 cells in 3D architecture had increased expression of p-STAT3 (control of numerous critical cellular processes, including cell proliferation, survival, and metastasis), p-p38 (cellular stress response), and puma (pro-apoptotic protein). Furthermore, decreased expression of p-Akt (cell growth, proliferation, migration, and survival), p-ERK (differentiation, proliferation, and apoptosis), p-FAK (differentiation, cell spreading, and migration), MYLK (migration), anti-apoptotic proteins (Mcl-1 and survivin), and cell cycle regulators (cyclin D1, cyclin D3 and CDK2) was observed in A549 cells in 3D culture compared with those in 2D cells.

STAT3 inhibitor sensitizes A549 cells cultured in 3D microenvironment towards doxorubicin and etoposide-mediated cytotoxicity. Western blot analysis indicated an increased expression level of p-STAT3 and decreased levels of p-ERK and p-Akt, three key signaling molecules involved in numerous biological activities. Specific inhibitors of STAT3 (CBC-I), MEK1/2 (U0126), and PI3K (LY-294002) were used to study the correlation between these signaling nodes and dormancy, as well as chemoresistance. The inhibitor doses were chosen to have least impact on cell viability (with over 80% cell survival). Thus, after treatment of A549 cells in 3D culture with 25 nM of CBC-I and treatment of 2D monolayer cells with 30 μM of U0126 or 20 μM of LY-294002 for 24 h prior to and during the assays, cell cycle progression and chemosensitivity to doxorubicin and etoposide (the most resistant drugs in the present study) were evaluated. Doxorubicin and etoposide are well-known chemotherapeutic agents. Although not centrally used in NSCLC, the combination of etoposide and platinum-based anticancer drug has been studied for efficacy and safety in the treatment of lung cancer (26). The combination of lurbinectedin and doxorubicin is being tested as second-line therapy in a phase III trial (27) and the combination of photodynamic therapy and doxorubicin has been shown to improve long-term lung cancer cure rates (28). The results showed that inhibitors of ERK and Akt shifted the cell cycle distribution of 2D cells toward G_0/G_1 phase arrest (75.6±3.1 and 70.5±2.8% for U0126 and LY-294002 treatment, respectively; Fig. 4). These inhibitors also decreased susceptibility to the cytotoxic effects of doxorubicin [cells treated with U0126 or LY-294002 had IC_{50} values of 2.4±0.1 μM (3.2-fold) and 2.1±0.0 μM (2.7-fold), respectively; Fig. 7] and etoposide [the IC_{50} values for cells treated with U0126 or LY-294002 were 255±22.7 μM (10.7-fold) and 174±16.4 μM (7.2-fold), respectively; Fig. 7]. The STAT3 inhibitor, although showing little to no effect on the cell cycle (71.6±3.1% for G_0/G_1 phase; Fig. 4), substantially increased doxorubicin and etoposide cytotoxicity to levels comparable to those of the corresponding 2D cells [IC_{50} values were 0.9±0.1 μM (1.1-fold) and 40.2±5.2 μM (1.7-fold) for doxorubicin and etoposide, respectively; Fig. 7]. These results highlighted the importance of p-STAT3 on doxorubicin and etoposide resistance of A549 cells cultured in 3D.

Discussion

The large gap between studies using the 2D culture model and the results from *in vivo* environment indicates the lack of a

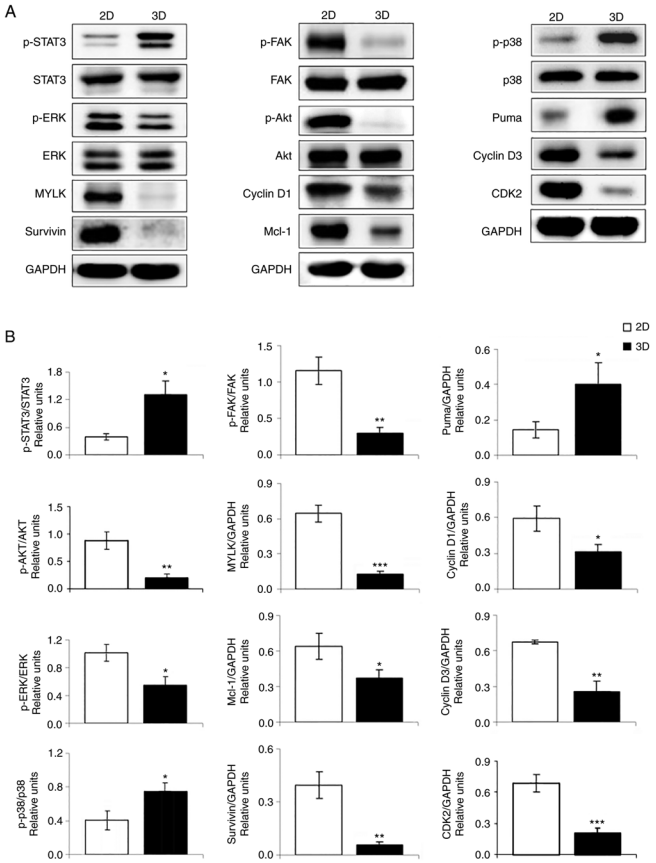

Figure 6. Western blotting and quantitative analysis of protein expression profiles of A549 cells in 2D/3D culturing systems. (A) Representative blots and (B) relative levels of the expression of proteins related to cell growth, proliferation, survival, cellular stress, migration, apoptosis and cell cycle regulation from at least three independent experiments. Expression of proteins in the phosphorylated states was normalized with respect to the non-phosphorylated counterparts. The loading control (GAPDH) served as the baseline for all other proteins. *P<0.05, **P<0.01 and ***P<0.001 vs. 2D. p-, phosphorylated.

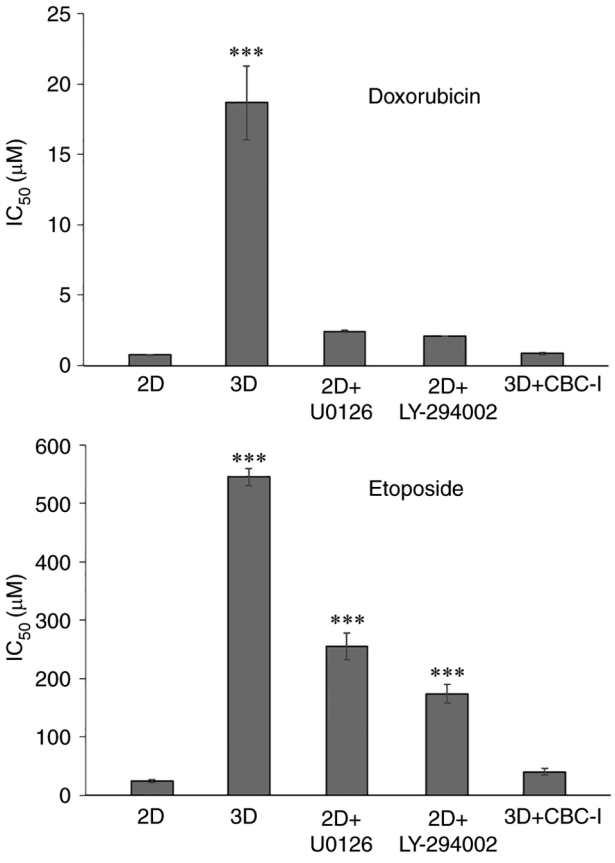

Figure 7. Effects of specific inhibitors (U0126, LY-294002 and CBC-I) on doxorubicin and etoposide chemosensitivity. A549 cells cultured in 2D condition were pre-incubated with U0126 (30 μM) or LY-294002 (20 μM), whereas cells cultured in 3D condition were pre-incubated with CBC-I (25 nM) 24 h prior to and during the drug sensitivity assay. Following treatment with various concentrations of doxorubicin and etoposide for 48 h, the degree of cell survival was measured using MTT assay. ***P<0.001 vs. 2D.

predictive preclinical model. Accumulating research has found that drug responses of cells in the 2D monolayer culture model do not accurately predict clinical study outcomes (29,30). As a consequence, numerous novel chemotherapeutic agents, that show promising results in 2D culture, fail during clinical trials (31,32). Given the relatively high failure rate of the 2D culture model in drug discovery and development, 3D culture platforms were developed to provide a higher degree of similarity to *in vivo* conditions. Previous experiments have shown that cells in 3D culture more closely imitate cell behavior, proliferation rate, gene or protein expression profiles, signaling and cellular responses found in living tissues and tumors, compared with their 2D counterparts (14,33). A previous study demonstrated that 3D cultures of epithelial ovarian cancer cells accurately reflect the biological, histological and molecular characteristics of primary tumors *in vivo* and in xenografts than traditional 2D cell cultures (34). Earlier studies indicated that, in terms of signaling, tumor cells undergoing 3D culture mimic *in vivo* tumor biology in an improved way compared with 2D monolayer culture model (35). As a result of greater *in vitro*-to-*in vivo* correlations, 3D cell culture gained attention in bridging the gap between traditional 2D monolayer and animal models, and more precisely predicting therapeutic efficacy of drug candidates.

In contrast to the 2D culture microenvironment where all cells receive uniformly rich nutrition and oxygenation, 3D cultures develop gradients of nutrients, oxygen, metabolites and waste. Therefore, proliferative gradients are established within the 3D aggregates with proliferating cells found mainly at the outer surface (24), while quiescent, hypoxic, necrotic or apoptotic cells occur at the core of the spheroid due to the restricted nutrients, growth factors, and oxygen (36). This cellular heterogeneity, a feature resembling *in vivo* tissues and tumors, was found in A549 cells cultured in 3D culture of the present study. Annexin V staining and flow cytometry-based apoptosis detection indicated increased apoptosis in A549 cells under 3D-culture compared with the 2D-cultured counterparts. A similar finding was reported by Mishra *et al* (37), who showed a significantly higher Caspase-3 staining of cells cultured in the *ex vivo* 3D model than in the 2D culture. Higher expression of a pro-apoptotic protein, puma, concurrently with the decreased levels of anti-apoptotic proteins, Mcl-1 and survivin, observed in 3D cultures by western blot analysis further support this notion. Consistent with these data, the hypoxic states of the cells in 3D architecture were detected using RT-qPCR, which revealed an increase in HIF-1a, the master transcriptional regulator of hypoxia responses, levels.

It has previously been reported that in order to maintain homeostasis, cells at the core of spheroids adapt their metabolism and become quiescent prior to cell death (38). A previous study by the authors indicated that these non-proliferating quiescent/dormant cells residing in the G_0/G_1 phase could avoid cell death induced by chemotherapeutic agents (22). Cell cycle distribution analysis of the present results revealed that A549 cells cultured in 3D induced G_0/G_1 cell cycle arrest, which could be responsible for the acquired chemoresistance. It is well documented that cyclin D-CDK4, cyclin D-CDK 6, and cyclin E-CDK2 complexes are essential cell cycle machinery components which govern transition from G_1 to S phase (39). In the present study, the decreased levels of cyclin D1 and cyclin D3 were observed in A549 cells cultured in 3D, together with the decreased CDK2 levels, so that the progression through the G_1 phase was halted. It is evident that the ERK to p38 activity ratio can be used to as a determinant of *in vivo* cell proliferation or dormancy (40). ERK has been demonstrated to be negatively regulated by p38 and the high p38/ERK ratio favors growth arrest (40), consistent with the reduction in ERK1/2 activation and the enhanced phosphorylation of p38 observed in 3D aggregates of A549 cells.

3D-cultivation of A549 cells caused a marked decrease in p-FAK and MYLK, the two important mediators for cell migration, expression (by western blotting), concurrent with the decreased levels of a panel of beta-tubulin, the building blocks of microtubules, (by RT-qPCR) which was also implicated in cell migration. This is in line with the decrease in migration capability of A549 cells undergoing 3D culture. Numerous studies have shown that beta-tubulin is functionally linked to cell migration; for example, Kanojia *et al* (41) demonstrated the overexpression of TUBBIII in breast cancer brain metastases and the critical role of TUBBIII in metastatic ability *in vivo*. A large body of evidence now supports the significance of uPA and c-Met, a receptor tyrosine kinase, in cancer invasion and metastasis (42,43). Moreover, Lim *et al* (44) have shown that c-Met promoted cancer cell migration and invasion through MMP-1, MMP-2 and MMP-9 expression. These findings were in consistency with the results of the present study, which showed decreased invasion rate of A549 cells in 3D microenvironment that corresponded with the decreased levels of uPA, c-Met, MMP-2 and MMP-9. The family of TIMPs (TIMP-1 to TIMP-4) play a key role as specific inhibitors of MMPs. Notably, Hernandez-Barrantes *et al* (45) revealed that TIMP-2 has dual roles, serving as both an MMP inhibitor and a positive regulator of MMP-2 activity. This was consistent with the decrease in TIMP-2 and an increase in TIMP-1 and TIMP-4 mRNA levels observed in the present study.

An abundance of evidence indicates that cancer stem cells (CSCs), a subpopulation of cancer cells with stem-like properties, have been strongly implicated in tumor initiation, chemoresistance, metastasis, and relapse (46). In the present study, RT-qPCR analysis results revealed a marked increase in the expression levels of several stem cell markers, including Oct4B, Nanog, CD133 and EPCAM, suggesting that A549 cells acquired stem-like properties due to 3D cultivation. Emerging data showed significant overlap between quiescent/dormant cells and CSCs, in terms of immune escape, quiescence and therapy resistance (47). Accumulated evidence has suggested that the resistance to antiproliferative chemotherapy of CSCs may be mediated by the relative quiescence (48). These data highlight the observation that A549 cells in 3D culture and CSCs share certain characteristics, including stemness marker expression, dormancy, and chemotherapeutic resistance.

Drug penetration is a critical parameter influencing response to therapy of cells in 3D culture system. In contrast to 2D cells that are equally exposed to drugs, diffusion is limited in 3D cells. However, the 3D cultured cells in the present study were disaggregated into single cells before exposure to anticancer agents, to allow drugs to fully penetrate the cells. The difference in chemosensitivity observed between cells in the 2D and 3D microenvironments was thus an intrinsic property of the cells *per se*. In addition to the proliferative status of the cells, the increased resistance to different classes of chemotherapeutic drugs of cells in 3D architecture could be due to hypoxia, which has been reported to play a major role in radio-/chemo-resistance (49). This supports the observation that A549 cells in 3D model demonstrated hypoxia and increased chemoresistance compared with 2D culture. The ATP-binding cassette (ABC) transporter represents the ATP-driven efflux pump superfamily that transports a wide variety of substrates across cell membranes. Concrete evidence indicates that the MDR-1 (ABCB1, ABC subfamily B member 1), plays a critical role in drug efflux transport and the emergence of drug resistance (50). MRPs (ABCC, ABC subfamily C) have been strongly implicated as determinants of multidrug resistance in cancer cells (51). Furthermore, LRP has been shown to be associated with drug resistance in acute myeloid leukemia (52). In support of a role for MDR-1, MRPs, and LRP in drug resistance, the present results revealed significantly higher levels of MDR-1, MRP-2, MRP-3 and LRP mRNA expression, which may act in concert with each other to confer drug resistance.

MAPK/ERK, PI3K/Akt, and STAT3, the three major cancer-associated pathways, are responsible for a wide range of cellular activities. Specific inhibitors of p-ERK, p-Akt and p-STAT3 were thus used for delineating the signaling pathway underlying increased drug resistance in 3D aggregates. In agreement with another study showing that MEK and PI3K inhibitors inhibited malignant pleural mesothelioma cell growth by inducing G_1 cell cycle arrest (53), the 2D-cultured cells in the current study experience quiescence and become more resistant to doxorubicin and etoposide, after being treated with specific MEK and PI3K/Akt inhibitors. However, the level of resistance was not comparable to that of cells cultured in the 3D manner, suggesting that the enhanced chemoresistance of 2D cells treated with specific inhibitors was most likely due to cell cycle arrest, since active cell proliferation is required for antiproliferative agents such as doxorubicin and etoposide. More importantly, the STAT3 inhibitor reverses doxorubicin and etoposide resistance in 3D-cultured A549 cells, underlining the critical role of p-STAT3 in mediating drug resistance. The JAK/STAT3 pathway has been implicated in enhanced resistance to a wide range of targeted cancer therapies and chemotherapies (54). This was consistent with a recent study showing that JAK/STAT3 suppression counteracts the cancer-associated fibroblast-induced chemoresistance of gastric cancer cells (55). A previous study has linked the STAT3 signaling pathway to the expression of multidrug resistance proteins such as MDR-1, MRPs and BCRP (56), which further supports the findings of the current study. A recent

study demonstrated that JAK/STAT3/PD-L1 pathway has been associated with ATM-mediated cisplatin-resistance, epithelial-to-mesenchymal transition and metastatic potential of lung cancer cells (57). Parallel research using a 3D microfluidic platform revealed that growth factors in the TME can provide a survival advantage and modulate chemoresistance in tumor cells. CAF-derived HGF was found to activate Met/PI3K/AKT, upregulate GRP78 and inhibit paclitaxel-induced apoptosis in A549 cells (58). A similar study found a link between the PI3K/Akt pathway, occludin expression and resistance to anticancer drugs in an A549 spheroid culture model (59).

As cancer therapeutics shift toward molecularly targeted therapies, which are drugs designed to block specific molecules involved in carcinogenesis, tumor growth and metastasis, highlight the importance of 3D culture systems for discovering new targets that conventional 2D cultures do not reveal. Immune checkpoint therapies have represented a cancer treatment breakthrough by preventing inhibitory checkpoint proteins from interacting with their partner proteins, thereby restoring cytotoxic T cell activity to attack cancer cells. Notably, currently approved immune checkpoint inhibitors such as PD-1, PD-L1 and CTLA-4 have been used to treat a variety of cancers (60). Although checkpoint blockade immunotherapy is a promising therapeutic strategy, the use of immune checkpoint inhibitors as monotherapy remains limited due to an unsatisfactory therapeutic effect. Furthermore, additional research has revealed that molecular targeted agents have immunostimulatory or immunosuppressive properties that impair therapeutic efficacy (61). As a result, combining molecularly targeted therapies with immune checkpoint therapies could be a potentially effective strategy for improving therapeutic responses. Indeed, various combination strategies are being investigated and have demonstrated significant synergistic treatment efficacy (62).

Cancer is a heterogeneous disease and cancer heterogeneity has long been recognized to play a significant role in treatment response. Cells cultured in 3D capture the heterogeneous nature of cancer biology while also preserving other key characteristics such as the highly complex 3D arrangement and the restoration of important microenvironmental cues. Although the 3D aggregates were not uniformly sized, the rates of reproducibility were quite high, as evidenced by the drug sensitivity results. The presence of proliferative and metabolic gradients in 3D aggregates, as well as restricted nutrition and oxygenation, mimics the *in vivo* microenvironment in an improved way and represents a significant improvement of 3D cultures over conventional 2D models. Furthermore, when compared with animal models, 3D culture systems are simple, fast, cost-effective and can reduce ethical concerns. However, 3D culture systems do not fully imitate the *in vivo* complexity of tumors. Current 3D models lack the complex vascular systems that provide nutrients, oxygenation and waste removal, and thus only represent the environment of avascular tumors. Moreover, their high costs in comparison to 2D cultures may be one of the practical challenges to their use as a routine approach in preclinical drug development. The present study adopted a model system that allowed cell-cell and cell-ECM interactions to mimic the complex *in vivo* architecture and microenvironment. However, one of the limitations to the present study is that the molecular targets and mechanisms underlying chemoresistance were determined only in 3D-cultured A549 cells. The response of the cells may differ depending on the cell type. Some cells slow their proliferation rate, while others grow rapidly when they come into contact with ECM proteins. Additional studies are planned using more and different types of cancer cell lines.

In summary, the present study demonstrated that the STAT3 signaling pathway could be a key mechanism underlying the 3D culture-induced chemoresistance of A549 cells. STAT3-targeted inhibition is therefore proposed as a promising strategy for increasing the efficacy of chemotherapeutic agents in A549 cells under 3D culture. The differences in the cellular responses among culture conditions described in the current study underscores the importance of complex crosstalks established between cancer cells, neighboring cells, as well as the surrounding ECM that ultimately influence gene and protein expression. The current standard procedure for screening compounds in drug discovery begins with 2D cell culture tests and progresses to animal model tests, and finally clinical trials. However, drug responses in 2D culture tests do not accurately predict clinical study outcomes. Thus, before proceeding to animal testing, it may be advantageous to incorporate 3D studies into drug screening programs as *in vitro* alternatives. Data from 3D models could lead to more efficient animal testing and a reduction in the number of animals used. These findings strongly suggest the potential application of the 3D culture systems as *in vitro* alternatives for preclinical drug development.

Acknowledgements

Not applicable.

Funding

The present study was supported by the Thailand Science Research and Innovation (TSRI), Chulabhorn Research Institute (grant no. 36821/4274354).

Availability of data and materials

The datasets used and/or analyzed during the current study are available from the corresponding author on reasonable request.

Authors' contributions

SK designed the study, performed the experiments, interpreted the data and wrote the manuscript. TS and NO performed sample preparation and western blot analysis. LN performed RT-qPCR and wrote the manuscript. JS contributed to the conception of the work, supervised the study design, and corrected the manuscript. SK and LN confirm the authenticity of all the raw data. All authors read and approved the final manuscript.

Ethics approval and consent to participate

Not applicable.

Patient consent for publication

Not applicable.

Competing interests

The authors declare that they have no competing interests.

References

1. Sung H, Ferlay J, Siegel RL, Laversanne M, Soerjomataram I, Jemal A and Bray F: Global cancer statistics 2020: GLOBOCAN estimates of incidence and mortality worldwide for 36 cancers in 185 countries. CA Cancer J Clin 71: 209-249, 2021.
2. World Health Organization (WHO): Cancer. WHO, Geneva, 2022. https://www.who.int/news-room/fact-sheets/detail/cancer. Accessed February 3, 2022.
3. Jemal A, Siegel R, Ward E, Hao Y, Xu J and Thun MJ: Cancer statistics, 2009. CA Cancer J Clin 59: 225-249, 2009.
4. Savage P, Stebbing J, Bower M and Crook T: Why does cytotoxic chemotherapy cure only some cancers? Nat Clin Pract Oncol 6: 43-52, 2009.
5. Mansoori B, Mohammadi A, Davudian S, Shirjang S and Baradaran B: The different mechanisms of cancer drug resistance: A brief review. Adv Pharm Bull 7: 339-348, 2017.
6. Artykov AA, Belov DA, Shipunova VO, Trushina DB, Deyev SM, Dolgikh DA, Kirpichnikov MP and Gasparian ME: Chemotherapeutic agents sensitize resistant cancer cells to the DR5-specific variant DR5-B more efficiently than to TRAIL by modulating the surface expression of death and decoy receptors. Cancers (Basel) 12: 1129, 2020.
7. Kim YH, Shin EA, Jung JH, Park JE, Koo J, Koo JI, Shim BS and Kim SH: Galbanic acid potentiates TRAIL induced apoptosis in resistant non-small cell lung cancer cells via inhibition of MDR1 and activation of caspases and DR5. Eur J Pharmacol 847: 91-96, 2019.
8. Kim MS, Haney MJ, Zhao Y, Mahajan V, Deygen I, Klyachko NL, Inskoe E, Piroyan A, Sokolsky M, Okolie O, *et al*: Development of exosome-encapsulated paclitaxel to overcome MDR in cancer cells. Nanomedicine 12: 655-664, 2016.
9. Weaver VM, Fischer AH, Peterson OW and Bissell MJ: The importance of the microenvironment in breast cancer progression: Recapitulation of mammary tumorigenesis using a unique human mammary epithelial cell model and a three-dimensional culture assay. Biochem Cell Biol 74: 833-851, 1996.
10. Hanahan D: Hallmarks of cancer: New dimensions. Cancer Discov 12: 31-46, 2022.
11. Hanahan D and Coussens LM: Accessories to the crime: Functions of cells recruited to the tumor microenvironment. Cancer Cell 21: 309-322, 2012.
12. Bhadriraju K and Chen CS: Engineering cellular microenvironments to improve cell-based drug testing. Drug Discov Today 7: 612-620, 2002.
13. Ashworth A, Balkwill F, Bast RC, Berek JS, Kaye A, Boyd JA, Mills G, Weinstein JN, Woolley K and Workman P: Opportunities and challenges in ovarian cancer research, a perspective from the 11th Ovarian cancer action/HHMT Forum, Lake Como, March 2007. Gynecol Oncol 108: 652-657, 2008.
14. Gurski LA, Petrelli NJ, Jia X and Farach-Carson MC: 3D matrices for anti-cancer drug testing and development. Oncol Issues 25: 20-25, 2010.
15. Baharvand H, Hashemi SM, Kazemi Ashtiani S and Farrokhi A: Differentiation of human embryonic stem cells into hepatocytes in 2D and 3D culture systems in vitro. Int J Dev Biol 50: 645-652, 2006.
16. Amann A, Gamerith G, Huber JM, Zwierzina M, Hilbe W and Zwierzina H: Predicting drug sensitivity by 3D cell culture models. Memo 8: 77-80, 2015.
17. Huber JM, Amann A, Koeck S, Lorenz E, Kelm JM, Obexer P, Zwierzina H and Gamerith G: Evaluation of assays for drug efficacy in a three-dimensional model of the lung. J Cancer Res Clin 142: 1955-1966, 2016.
18. Takahashi Y, Hori Y, Yamamoto T, Urashima T, Ohara Y and Tanaka H: 3D spheroid cultures improve the metabolic gene expression profiles of HepaRG cells. Biosci Rep 35: e00208, 2015.
19. Wiśniewski JR, Vildhede A, Norén A and Artursson P: In-depth quantitative analysis and comparison of the human hepatocyte and hepatoma cell line HepG2 proteomes. J Proteomics 136: 234-247, 2016.
20. Lee GY, Kenny PA, Lee EH and Bissell MJ: Three-dimensional culture models of normal and malignant breast epithelial cells. Nat Methods 4: 359-365, 2007.
21. Keeratichamroen S, Lirdprapamongkol K, Thongnest S, Boonsombat J, Chawengrum P, Sornprachum T, Sirirak J, Verathamjamras C, Ornnork N, Ruchirawat S and Svasti J: JAK2/STAT3-mediated dose-dependent cytostatic and cytotoxic effects of sesquiterpene lactones from Gymnanthemum extensum on A549 human lung carcinoma cells. Oncol Rep 47: 6, 2022.
22. Keeratichamroen S, Lirdprapamongkol K and Svasti J: Mechanism of ECM-induced dormancy and chemoresistance in A549 human lung carcinoma cells. Oncol Rep 39: 1765-1774, 2018.
23. Livak KJ and Schmittgen TD: Analysis of relative gene expression data using real-time quantitative PCR and the 2(-Delta Delta C(T)) method. Methods 25: 402-408, 2001.
24. Khaitan D, Chandna S, Arya MB and Dwarakanath BS: Establishment and characterization of multicellular spheroids from a human glioma cell line; implications for tumor therapy. J Transl Med 4: 12, 2006.
25. Mehta G, Hsiao AY, Ingram M, Luker GD and Takayama S: Opportunities and challenges for use of tumor spheroids as models to test drug delivery and efficacy. J Control Release 164: 192-204, 2012.
26. Wang Z, Mai S, Lv P, Xu L and Wang Y: Etoposide plus cisplatin chemotherapy improves the efficacy and safety of small cell lung cancer. Am J Transl Res 13: 12825-12833, 2021.
27. Olmedo ME, Forster M, Moreno V, López-Criado MP, Braña I, Flynn M, Doger B, de Miguel M, López-Vilariño JA, Núñez R, *et al*: Efficacy and safety of lurbinectedin and doxorubicin in relapsed small cell lung cancer. Results from an expansion cohort of a phase I study. Invest New Drugs 39: 1275-1283, 2021.
28. Cacaccio JC, Durrani FA, Missert JR and Pandey RK: Photodynamic therapy in combination with doxorubicin is superior to monotherapy for the treatment of lung cancer. Biomedicines 10: 857, 2022.
29. Gomez-Roman N, Stevenson K, Gilmour L, Hamilton G and Chalmers AJ: A novel 3D human glioblastoma cell culture system for modeling drug and radiation responses. Neuro Oncol 19: 229-241, 2017.
30. Aljitawi OS, Li D, Xiao Y, Zhang D, Ramachandran K, Stehno-Bittel L, Van Veldhuizen P, Lin TL, Kambhampati S and Garimella R: A novel three-dimensional stromal-based model for in vitro chemotherapy sensitivity testing of leukemia cells. Leuk Lymphoma 55: 378-391, 2014.
31. Kola I: The state of innovation in drug development. Clin Pharmacol Ther 83: 227-230, 2008.
32. Zanoni M, Piccinini F, Arienti C, Zamagni A, Santi S, Polico R, Bevilacqua A and Tesei A: 3D tumor spheroid models for in vitro therapeutic screening: A systematic approach to enhance the biological relevance of data obtained. Sci Rep 6: 19103, 2016.
33. Giannattasio A, Weil S, Kloess S, Ansari N, Stelzer EH, Cerwenka A, Steinle A, Koehl U and Koch J: Cytotoxicity and infiltration of human NK cells in in vivo-like tumor spheroids. BMC Cancer 15: 351, 2015.
34. Lee JM, Mhawech-Fauceglia P, Lee N, Parsanian LC, Lin YG, Gayther SA and Lawrenson K: A three-dimensional microenvironment alters protein expression and chemosensitivity of epithelial ovarian cancer cells in vitro. Lab Invest 93: 528-542, 2013.
35. Edmondson R, Broglie JJ, Adcock AF and Yang L: Three-dimensional cell culture systems and their applications in drug discovery and cell-based biosensors. Assay Drug Dev Technol 12: 207-218, 2014.
36. Riffle S and Hegde RS: Modeling tumor cell adaptations to hypoxia in multicellular tumor spheroids. J Exp Clin Cancer Res 36: 102, 2017.
37. Mishra DK, Sakamoto JH, Thrall MJ, Baird BN, Blackmon SH, Ferrari M, Kurie JM and Kim MP: Human lung cancer cells grown in an ex vivo 3D lung model produce matrix metalloproteinases not produced in 2D culture. PLoS One 7: e45308, 2012.
38. Walenta S, Dötsch J, Bourrat-Flöck B and Mueller-Klieser W: Size-dependent oxygenation and energy status in multicellular tumor spheroids. Adv Exp Med Biol 277: 889-893, 1990.
39. Topacio BR, Zatulovskiy E, Cristea S, Xie S, Tambo CS, Rubin SM, Sage J, Kõivomägi M and Skotheim JM: Cyclin D-Cdk4,6 drives cell-cycle progression via the retinoblastoma protein's C-terminal helix. Mol Cell 74: 758-770.e4, 2019.

40. Aguirre-Ghiso JA, Estrada Y, Liu D and Ossowski L: ERK(MAPK) activity as a determinant of tumor growth and dormancy; regulation by p38(SAPK). Cancer Res 63: 1684-1695, 2003.
41. Kanojia D, Morshed RA, Zhang L, Miska JM, Qiao J, Kim JW, Pytel P, Balyasnikova IV, Lesniak MS and Ahmed AU: βIII-tubulin regulates breast cancer metastases to the brain. Mol Cancer Ther 14: 1152-1161, 2015.
42. Duffy MJ: The urokinase plasminogen activator system: Role in malignancy. Curr Pharm Des 10: 39-49, 2004.
43. Nan L, Qin T, Xiao Y, Qian W, Li J, Wang Z, Ma J, Ma Q and Wu Z: Pancreatic stellate cells facilitate perineural invasion of pancreatic cancer via HGF/c-Met pathway. Cell Transplant 28: 1289-1298, 2019.
44. Lim YC, Han JH, Kang HJ, Kim YS, Lee BH, Choi EC and Kim CH: Overexpression of c-Met promotes invasion and metastasis of small oral tongue carcinoma. Oral Oncol 48: 1114-1119, 2012.
45. Hernandez-Barrantes S, Shimura Y, Soloway PD, Sang QA and Fridman R: Differential roles of TIMP-4 and TIMP-2 in pro-MMP-2 activation by MT1-MMP. Biochem Biophys Res Commun 281: 126-130, 2001.
46. Lu KH, Chen YW, Tsai PH, Tsai ML, Lee YY, Chiang CY, Kao CL, Chiou SH, Ku HH, Lin CH and Chen YJ: Evaluation of radiotherapy effect in resveratrol-treated medulloblastoma cancer stem-like cells. Childs Nerv Syst 25: 543-550, 2009.
47. Talukdar S, Bhoopathi P, Emdad L, Das S, Sarkar D and Fisher PB: Dormancy and cancer stem cells: An enigma for cancer therapeutic targeting. Adv Cancer Res 141: 43-84, 2019.
48. Arai F and Suda T: Maintenance of quiescent hematopoietic stem cells in the osteoblastic niche. Ann N Y Acad Sci 1106: 41-53, 2007.
49. Olive PL and Durand RE: Drug and radiation resistance in spheroids: Cell contact and kinetics. Cancer Metastasis Rev 13: 121-138, 1994.
50. Fardel O, Payen L, Courtois A, Vernhet L and Lecureur V: Regulation of biliary drug efflux pump expression by hormones and xenobiotics. Toxicology 167: 37-46, 2001.
51. Korita PV, Wakai T, Shirai Y, Matsuda Y, Sakata J, Takamura M, Yano M, Sanpei A, Aoyagi Y, Hatakeyama K and Ajioka Y: Multidrug resistance-associated protein 2 determines the efficacy of cisplatin in patients with hepatocellular carcinoma. Oncol Rep 23: 965-972, 2010.
52. Pirker R, Pohl G, Stranzl T, Suchomel RW, Scheper RJ, Jäger U, Geissler K, Lechner K and Filipits M: The lung resistance protein (LRP) predicts poor outcome in acute myeloid leukemia. Adv Exp Med Biol 457: 133-139, 1999.
53. Miyoshi S, Hamada H, Hamaguchi N, Kato A, Katayama H, Irifune K, Ito R, Miyazaki T, Okura T and Higaki J: Antitumor activity of MEK and PI3K inhibitors against malignant pleural mesothelioma cells *in vitro* and *in vivo*. Int J Oncol 41: 449-456, 2012.
54. Resemann HK, Watson CJ and Lloyd-Lewis B: The Stat3 paradox: A killer and an oncogene. Mol Cell Endocrinol 382: 603-611, 2014.
55. Ham IH, Wang L, Lee D, Woo J, Kim TH, Jeong HY, Oh HJ, Choi KS, Kim TM and Hur H: Curcumin inhibits the cancer-associated fibroblast-derived chemoresistance of gastric cancer through the suppression of the JAK/STAT3 signaling pathway. Int J Oncol 61: 85, 2022.
56. Seo HS, Ku JM, Choi HS, Woo JK, Lee BH, Kim DS, Song HJ, Jang BH, Shin YC and Ko SG: Apigenin overcomes drug resistance by blocking the signal transducer and activator of transcription 3 signaling in breast cancer cells. Oncol Rep 38: 715-724, 2017.
57. Shen M, Xu Z, Xu W, Jiang K, Zhang F, Ding Q, Xu Z and Chen Y: Inhibition of ATM reverses EMT and decreases metastatic potential of cisplatin-resistant lung cancer cells through JAK/STAT3/PD-L1 pathway. J Exp Clin Cancer Res 38: 149, 2019.
58. Ying L, Zhu Z, Xu Z, He T, Li E, Guo Z, Liu F, Jiang C and Wang Q: Cancer associated fibroblast-derived hepatocyte growth factor inhibits the paclitaxel-induced apoptosis of lung cancer a549 cells by up-regulating the PI3K/Akt and GRP78 signaling on a microfluidic platform. PLoS One 10: e0129593, 2015.
59. Eguchi H, Akizuki R, Maruhashi R, Tsukimoto M, Furuta T, Matsunaga T, Endo S and Ikari A: Increase in resistance to anticancer drugs involves occludin in spheroid culture model of lung adenocarcinoma A549 cells. Sci Rep 8: 15157, 2018.
60. Archilla-Ortega A, Domuro C, Martin-Liberal J and Muñoz P: Blockade of novel immune checkpoints and new therapeutic combinations to boost antitumor immunity. J Exp Clin Cancer Res 41: 62, 2022.
61. Liu XD, Hoang A, Zhou L, Kalra S, Yetil A, Sun M, Ding Z, Zhang X, Bai S, German P, *et al*: Resistance to antiangiogenic therapy is associated with an immunosuppressive tumor microenvironment in metastatic renal cell carcinoma. Cancer Immunol Res 3: 1017-1029, 2015.
62. Kohlhapp FJ, Haribhai D, Mathew R, Duggan R, Ellis PA, Wang R, Lasater EA, Shi Y, Dave N, Riehm JJ, *et al*: Venetoclax increases intratumoral effector T cells and antitumor efficacy in combination with immune checkpoint blockade. Cancer Discov 11: 68-79, 2021.